



Capacity fading in lithium/sulfur batteries: A linear four-state model

Sebastian Risse ^{a,*}, Stefano Angioletti-Uberti ^{a,b}, Joachim Dzubiella ^{a,b},
Matthias Ballauff ^{a,b}

^a Helmholtz Zentrum Berlin (HZB), Institute of Soft Matter and Functional Materials, Hahn-Meitner Platz 1, 14109 Berlin, Germany

^b Humboldt University of Berlin, Institute of Physics, Unter den Linden 6, 10099 Berlin, Germany



HIGHLIGHTS

- We introduce a model for the analysis of capacity fading curves of Li/S cells.
- The model describes the discharge process as a Markov chain.
- This approach describes a broad variety of different systems.
- A direct comparison of different concepts of Li/S batteries is enabled.

ARTICLE INFO

Article history:

Received 10 March 2014

Received in revised form

7 May 2014

Accepted 14 May 2014

Available online 7 June 2014

Keywords:

Capacity fading model

Lithium/sulfur cell

Markov process

Linear four state model

ABSTRACT

Lithium/sulfur batteries represent a promising class of energy storage systems. Their drawback still preventing major technical applications is the fading of capacity with the number of cycles. Here we introduce a linear four state model that is capable of describing the majority of the capacity fading curves of recently presented Li/S battery systems with different cathode materials (e.g. carbon, metal oxide and metals). Our approach models the discharge process as a Markov chain and consists of only four states that belong to three phases. The living phase comprises a stable and unstable state. The sleeping phase is converted into the living stable state and the dead phase represents the irreversible loss of living phase during the charge/discharge process. Despite its inherent simplicity this approach describes a broad variety of different systems. It gives detailed insights into the fading mechanisms of lithium sulfur cells. Moreover, it represents an easy-to-use tool for the quantitative assessment of a given system in terms of three figures of merit.

© 2014 Elsevier B.V. All rights reserved.

1. Introduction

Lithium/sulfur (Li/S) batteries are discussed as a cost efficient key technology for future applications in portable electronic devices, electromobility and as a backup storage system for the reliable use of renewable energies [1–3]. Because of their high theoretical electrochemical capacity C_{ec}^{\max} of 1675 mAh g⁻¹ Li/S batteries represent in principle an efficient energy storage system. Moreover, the abundance and low-cost of their raw materials are important advantages of this battery concept. Hence, Li/S batteries have become the subject of an intense research with several publications per week. However, the pronounced capacity fading with

increasing cycle number has prevented so far a broad technical application of this system [4].

The decrease of the capacity with cycling is a well known problem for all types of batteries. Especially lithium-ion batteries have been the subject of intense research in order to elucidate the various reasons for the loss of capacity during usage. Thus, many models have been presented that deal with capacity fading of lithium-ion batteries [5–14]. In the review of Arora et al. [5] several causes for capacity fading processes were described in detail. Capacity fading models of Li-ion batteries focus on many parameters like temperature [11,7], growth of a solid electrolyte interface (SEI) layer [12,10,14], active material degradation [6,12,7] and solvent reduction [8]. Similar mechanisms of capacity fading may also be operative in Li/S batteries. However, up to now no model has been introduced that quantitatively analyzes the fading of capacity of Li/S batteries with the number of charge/discharge cycles. Evidently, a modeling of capacity fading in Li/S systems would be highly

* Corresponding author.

E-mail address: sebastian.risse@helmholtz-berlin.de (S. Risse).

URL: <http://www.helmholtz-berlin.de>

desirable inasmuch it would lead to a quantitative comparison between different materials or chemical processing routes.

Here, we introduce a linear four state model that can be used to analyze to the majority of the published capacity fading curves. Fig. 1 gives a survey of typical fading curves where the capacity is plotted as the function of the number of cycles. First of all, ordinary battery aging (curve a)) occurs in every real battery system and determines the long-term stability of the system. In addition to this curve b) and d) describe a film formation period at the electrodes and an additional activation of material, respectively. Curve c) represents a superposition of all processes. The model developed here allows us to analyze the complex processes in Li/S batteries leading to these characteristic fading curves. Based on the model we present three figures of merit that characterize a given Li/S battery.

Our model is based on a Markov process [15], that describes the evolution of the fractions f_i of the system in each state after one charge/discharge cycle, given the present composition. This theory is widely applied to model processes in structural biology [16,17], to optimize the power management of devices and electric vehicles [18–20] or to solve optimization problems in energy supply [21]. It was also previously used to describe a battery's degradation process in the context of implementing optimal power management schedules for devices and electric vehicles. These models typically assume a specific chemical system, and then model degradation based on this assumption [18,22]. Our aim is different. What we are about to show is that a large variety of cathode materials, differing both in terms of chemical composition as well as the specific route followed for their synthesis, show degradation properties that can be described within a unifying framework using a simple Markov model. Since the parameters' in this model can be linked to known physicochemical degradation processes and materials properties, our model aims to provide a qualitative and quantitative tool to evaluate how various design choices might eventually affect a battery's life. To the best of our knowledge, no previous simple and general model was shown to achieve such goal.

The linear four state model developed here is applied to the three typical Li/S systems that differ with regard to their cathode material. Specifically, the cathode of the respective systems is made from either carbon [23,24], a metal oxide composite [25,26], or a metal composite [27]. Metals and metal oxides have been introduced in order to achieve a successful confinement of polysulfides. The strongest adsorption (chemisorption) of sulfur occurs on metal surfaces followed by metal oxides. This fact is reflected by the effect of poisoning of catalysts by sulfur [28]. On the other hand, carbon surfaces exhibit only weak interaction with sulfur (physisorption).

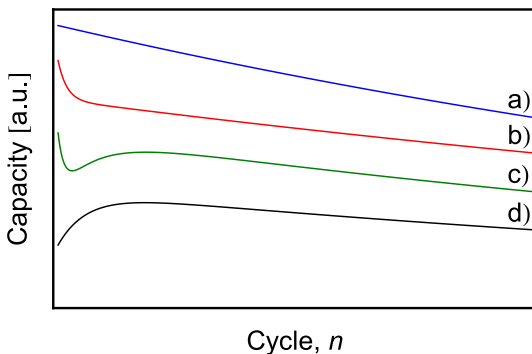


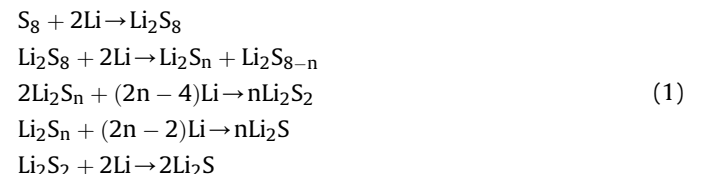
Fig. 1. Capacity fading of lithium/sulfur batteries: The capacity of a Li/S system is plotted as the number of discharge/charge cycles. Here we plot four typical fading curves that apply to practically all published data. The model developed here allows us to discern the different decay channels in Li/S systems.

We demonstrate here that the confinement of the polysulfides can directly be correlated to parameters deriving from our model.

2. Model

The model which is shown in Fig. 2 consists of only four states that belong to three phases. First, the living phase comprises a stable $f_{\text{liv}1}$ and unstable $f_{\text{liv}2}$ state. Both fractions contribute to the electrochemical capacity of the battery. Second, a sleeping phase f_s that is converted into the living stable state with increasing cycle number. Third, a dead phase f_d that represents the irreversible loss of living phase which cannot contribute to the charge/discharge process anymore. Transitions between these four states are governed by three conditional transition probabilities $k_{\text{liv}1 \rightarrow d}$, $k_{\text{liv}2 \rightarrow d}$ and $k_{s \rightarrow \text{liv}1}$.

The majority of the capacity curves presented are normalized with respect to the mass of sulfur that is employed in the Li/S battery. Therefore the maximum capacity during the discharge is limited to $C_{\text{ec}}^{\max} = 1675 \text{ mAh g}^{-1}$ of sulfur. The fraction of living phase f_{liv} in our model can be regarded as the part of sulfur and lithium-ions that participate in the sulfur reduction process (i.e., in the battery's discharge) (Eq. (1)). Therefore the measured battery capacity is the product of f_{liv} and C_{ec}^{\max} .



If high amounts of one reaction partner in the sulfur reduction process (Eq. (1)) are irreversibly fixed in other chemical compounds (e.g. SEI-layer, the passivation layer, insoluble salts) f_{liv} decreases. The unusable or inaccessible amounts of Li and S are assigned to the dead phase f_d of the battery. Finally, the sleeping phase f_s represents a state that can be converted into the stable living phase during cycling.

The majority of Li/S cells exhibit a sharp decay in electrochemical capacity at the beginning of the cycling process [5]. This process has been attributed to the film formation of e.g. a SEI layer or an electrode passivation layer during the early cycling periods [5]. Formation of these films are caused by electrolyte decomposition and unwanted side reactions of the polysulfide or lithium ions in the vicinity of both electrodes' surfaces. After all available electrode surfaces are coated, this reaction stops. In order to account for this process, we assume that there are two living phases, namely $f_{\text{liv}1}$ and $f_{\text{liv}2}$. Here the latter represents the amount of living phase necessary for the initial film formation, which transforms to the dead phase f_d with a conditional transition probability $k_{\text{liv}2 \rightarrow d}$. This fraction cannot contribute to the electrochemical capacity

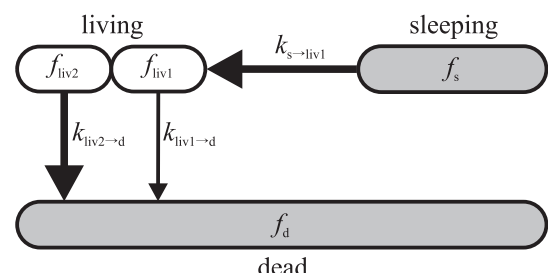


Fig. 2. Linear four state model describing the transition of different phases during cycling of Li/S batteries.

anymore. The other living phase $f_{\text{liv}1}$ represents a more stable state that have a much lower transition probability $k_{\text{liv}1 \rightarrow d}$ than the amount that is consumed during the initial period. Batteries with a high value of $f_{\text{liv}1}$ are characterized by long cycle life.

In particular, the formation of a SEI-layer at the cathode plays an important role for the reduction process of sulfur. If the SEI film supports the conductivity of Li^+ or e^- more sulfur phase can be accessed after the formation of this layer. Thus, a phase that was previously inactive is converted into a living phase. We call this inactive phase the sleeping phase f_s , which increases the battery capacity by transforming into $f_{\text{liv}1}$ with a conditional transition probability $k_{s \rightarrow \text{liv}1}$. In the interest of simplicity it is assumed that the sleeping phase is rapidly converted only to the stable living state $f_{\text{liv}1}$ to avoid the introduction of additional parameters.

These transitions shown in Fig. 2 and the underlying evolution of the system can be described using a Markov chain model [29]. In such a model the evolution of a system depends only on its current state. At every step (in our case, a battery's cycle), each phase A is converted to phase B with a probability given by $P(A \rightarrow B|A)P(A)$, where $P(A) \equiv f_A$ is the probability of finding the system in state A (or, in other words, the fraction of the system in state A) and $P(A \rightarrow B|A) \equiv k_{A \rightarrow B}$ is the conditional probability that the system evolves from A to B given that it is currently in state A .

The evolution of the system can thus be represented by a 4×4 transition matrix T , the entries of which are shown in Eq. (2).

$$T = \begin{pmatrix} 1 - k_{\text{liv}1 \rightarrow d} & 0 & k_{s \rightarrow \text{liv}1} & 0 \\ 0 & 1 - k_{\text{liv}2 \rightarrow d} & 0 & 0 \\ 0 & 0 & 1 - k_{s \rightarrow \text{liv}1} & 0 \\ k_{\text{liv}1 \rightarrow d} & k_{\text{liv}2 \rightarrow d} & 0 & 1 \end{pmatrix} \quad (2)$$

The state of the system at cycle n is represented by a column vector of which entries are the fraction of the 4 different phases $\vec{f}_n = \{f_{\text{liv}1}(n), f_{\text{liv}2}(n), f_s(n), f_d(n)\}^T$. The state vector is mapped from the n th cycle to the next one $n+1$ by applying T (Eq. (3)), i.e.:

$$T \vec{f}_n = \vec{f}_{n+1} \text{ with } \vec{f}_0 = \begin{pmatrix} f_{\text{liv}1} \\ f_{\text{liv}2} \\ f_s \\ f_d \end{pmatrix} \quad (3)$$

By construction, the sum of the elements in each column is 1, and all its elements are non-negative (i.e. $\forall t_{ij} \in T_{ij} \geq 0$). Hence T is a (left) stochastic matrix and possesses a few important characteristics describing the evolution of the system. First of all, the sum of all entries in the state vector is a conserved quantity, reflecting mass conservation in our process. Second of all, all four eigenvalues ϵ_i of the matrix T are between zero and one, and one of them, which we call ϵ_4 is exactly equal to one. Re-writing the initial state vector $\vec{f}(0)$ using the eigenvectors basis $\{\vec{u}\}$ and applying Eq. (3) n times, one thus obtains:

$$\vec{f}_n = T^n \vec{f}_0 = \quad (4)$$

$$\sum_i \alpha_i(0) \epsilon_i^n \vec{u}_i \quad (5)$$

where the sum i is extended over all four eigenvectors, T^n is a short-hand notation for the repeated application of T n times, and the α_i are the projections of the initial state on the eigenvector basis. Since all ϵ_i but the last are smaller than one and positive, Eq. (5) shows that the system tends asymptotically to:

$$\lim_{n \rightarrow \infty} \vec{f}_n = \alpha_4(0) \vec{u}_4 \quad (6)$$

Hence, \vec{u}_4 represents the final, stable state of the system, regardless of the starting composition. This eigenvector is the

column vector $\{0, 0, 0, 1\}^T$, which represents a system where the only phase present is the dead phase. This is to be expected since there is an irreversible, i.e. unidirectional, path connecting all phases to the dead phase and all components will eventually transform to it and remain there. We note that the sum of the first two entries in \vec{f}_n represents the living phase and therefore yields the expected electrochemical capacity $C_{\text{ec}}(n)$ when multiplied by the maximum value $C_{\text{ec}}^{\max} = 1675 \text{ mAh g}^{-1}$. By applying standard matrix diagonalization together with Eq. (4), the state of the system after n cycles can be shown to be given by:

$$\vec{f}(n) = SD^n S^{-1} \vec{f}(0). \quad (7)$$

D^n is the n th power of the diagonal matrix whose entries are the eigenvalues of T . D^n is thus itself diagonal and its only non-zero entries are $d_{ii}^n = \epsilon_i^n$. Finally, S is a matrix where column is one of the eigenvectors of T , and S^{-1} is its inverse [30].

$$C_{\text{ec}}(n) = C_{\text{ec}}^{\max} \left[f_{\text{liv}1}(1 - k_{\text{liv}1 \rightarrow d})^n + f_{\text{liv}2}(1 - k_{\text{liv}2 \rightarrow d})^n \right. \\ \left. + \frac{f_s k_{s \rightarrow \text{liv}1}}{k_{s \rightarrow \text{liv}1} - k_{\text{liv}1 \rightarrow d}} ((1 - k_{\text{liv}1 \rightarrow d})^n - (1 - k_{s \rightarrow \text{liv}1})^n) \right] \quad (8)$$

Eq. (8) can be rewritten in a slightly more compact form by making the following substitutions

$$k_{\text{liv}1 \rightarrow d} = 1 - e^\alpha \\ k_{\text{liv}2 \rightarrow d} = 1 - e^{\alpha+\beta} \\ k_{s \rightarrow \text{liv}1} = 1 - e^{\alpha+\gamma} \quad (9)$$

where α , β and γ are three dimensionless constants. Using Eq. (9), we thus obtain:

$$C_{\text{ec}}(n) = C_{\text{ec}}^{\max} e^{\alpha n} \left[f_{\text{liv}1} + f_{\text{liv}2} e^{\beta n} + f_s (1 - e^{\gamma n}) \frac{1 - e^{\alpha+\gamma}}{e^\alpha - e^{\alpha+\gamma}} \right] \quad (10)$$

In conclusion, the whole system can be described by three exponential functions with different dimensionless constants (α , β , γ) and three starting values ($f_{\text{liv}1}$, $f_{\text{liv}2}$, f_s).

To assess the battery performance of the Li/S systems under consideration here three figures of merit are introduced. One important point for the application of energy storage devices is their reliability with respect to their energy output rate. Therefore the first assessment parameter is the cycle number $n_{1/2}$ at which the electrochemical capacity $C_{\text{ec}}(n)$ has reached half of its initial value ($\frac{1}{2}C_{\text{ec}}(1)$) (Eq. (11)). Batteries that exhibit a very high $n_{1/2}$ have a small value of $k_{\text{liv}1 \rightarrow d}$ and exhibit a nearly constant energy output after each charging. In addition, battery systems should exhibit high values of the stable living phase $f_{\text{liv}1}$. Therefore the second assessment criteria is the average electrochemical capacity of the battery in the range between the first and $n_{1/2}$ th cycle (Eq. (12)).

$$n_{1/2} : \frac{1}{2} C_{\text{ec}}(1) = C_{\text{ec}}(n_{1/2}) \quad (11)$$

$$\overline{C_{\text{ec}}} : \overline{C_{\text{ec}}} = \frac{1}{n_{1/2}} \sum_{i=1}^{n_{1/2}} C_{\text{ec}}(i) \quad (12)$$

The product of $n_{1/2}$ and $\overline{C_{\text{ec}}}$ gives the overall charge output C_{tot} of the battery system and represents the third figure of merit.

3. Results and discussion

The four state model derived above was used to analyze several electrochemical capacity curves [23–27]. As mentioned above, the choice of these systems was motivated by their different cathode materials. Because their light weight and versatile structure, carbon cathodes are the most intensively studied material for Li/S batteries [24,23]. Metal oxide (e.g. Al_2O_3 , TiO_2) encapsulated sulfur [25,26] is another promising concept for the confinement of polysulfides due to the strong surface interaction between sulfur and metal atoms [28]. This strong chemisorption of soluble sulfur species is also dominant in the third group that deals with partly metallic cathodes [27]. In the following we present the analysis of these three systems and the consequences for their possible use as battery materials.

3.1. Carbon cathodes

Sun et al. [23] investigated the influence of nitrogen doping on the cyclability of sulfur loaded mesoporous carbon cathodes in lithium sulfur cells. In this work sulfur loading was achieved by the catalytic oxidation of H_2S on mesoporous carbon framework and melting impregnation. The cyclic measurements were performed with 60 wt% sulfur content and a charge/discharge rate of 0.2C. The improvements in this work are, first, a nitrogen-enriched carbon framework and, second, the catalytic oxidation meaning a layer-by-layer sulfur deposition that allows atomic sulfur to bind strongly with the carbon framework. This provides an efficient immobilization of sulfur. The results of this concept were successively shown using three different samples (Fig. 3).

The fit of the four state model to the data in Fig. 3 demonstrates a good agreement between model and measurement. The model parameters are summarized in Table 1. Both concepts, namely the nitrogen-enriched carbon and the catalytic oxidation, lead to a significant enhancement of cyclability. The amount of $f_{\text{liv}1}$ that characterizes a long cyclability is increased while the unstable living state $f_{\text{liv}2}$ that is rapidly converted from the living to the dead phase decreases. Also the conditional transition probability $k_{\text{liv}1 \rightarrow d}$ is decreased by more than 70% from MC-MI to NMC-CO resulting in an enhanced life time of the stable living phase. The occurrence of a sleeping phase (f_s) was not detected. Hence, this system shows a satisfying performance with a half life cycle number $n_{1/2}$ of more than 500 and an average capacity C_{ec} of 748 mAh g^{-1} .

Kazazi et al. investigated the cyclability of sulfur coated multi-wall carbon nanotubes. Compared to the conventional system,

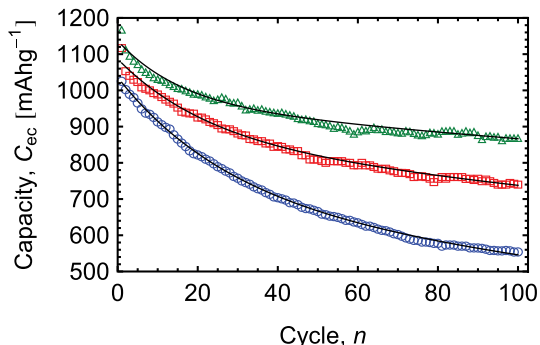


Fig. 3. Cycle dependent electrochemical capacity taken from the work of Sun et al. [23]. Sulfur content 60 wt%, charge/discharge rate 0.2C. \circ : Mesoporous carbon with sulfur melting impregnation (MC-MI), \square : Nitrogen enriched mesoporous carbon with sulfur melting impregnation (NMC-MI), \triangle : Nitrogen enriched mesoporous carbon with catalytic oxidation sulfur deposition (NMC-CO).

they applied an additional polypyrrole coating to the nanotubes in order to suppress the diffusion of lithium polysulfide. Furthermore they demonstrated the effect of different charging rates r_C on the cycle dependent electrochemical capacity. A value of $r_C = 1\text{C}$ corresponds to a charge/discharge current of $I = 1675 \text{ mA g}^{-1}$ sulfur (i.e. a charge/discharge duration of 1 h).

The discharge/charge rates between 0.06C and 3C have a significant influence on the electrochemical capacity (Fig. 4, top). The higher the rate the lower the obtained capacity. All fitting curves show a good agreement between data and model.

The change in C_{ec} that depends on the cycling rate is reflected by the model parameters (Fig. 4 bottom, w/o PPy). Both living phases $f_{\text{liv}1}$ and $f_{\text{liv}2}$ increase with decreasing cycling rate while the conditional transition probability $k_{\text{liv}1 \rightarrow d}$ decreases for decreasing cycling rates. The rate dependence of the living phase could be explained by the reaction kinetics of the sulfur reduction process. A higher amount of the living phase can finish the reduction process only at sufficiently long cycle duration. The same argumentation is valid for the parameter $k_{\text{liv}1 \rightarrow d}$ that represents the irreversible loss of living phase by undesirable side reactions. Also these parasitic reactions are favored if sufficient time is provided. Finally, the carbon-based cathode system does not exhibit a sleeping phase.

In a next step, the same authors applied an additional polypyrrole coating to the nanotubes (Fig. 4, bottom). It can be seen that all curves are shifted to higher electrochemical capacities. The increase in living phase, $f_{\text{liv}1}$ and $f_{\text{liv}2}$ with decreasing cycling rate r_C can be observed again (Fig. 4 bottom, with PPy). However, compared to the system without polypyrrole coating the values of $f_{\text{liv}1}$ are enhanced and the unstable living phase $f_{\text{liv}2}$ is decreased. Also the conditional transition probabilities $k_{\text{liv}1 \rightarrow d}$ are decreased, representing a better cycle stability. Furthermore, the dependence of $k_{\text{liv}1 \rightarrow d}$ on the charge/discharge rate is not so pronounced anymore. Therefore it can be concluded that the presence of a conductive polypyrrole coating has positive effects on sulfur reduction kinetics and possibly diminishes the occurrence of parasitic side reactions. A sleeping phase f_s is also not detected for this battery system.

3.2. TiO_2 cathodes

Ding et al. [25] used the encapsulation of sulfur phase with TiO_2 . In this work sulfur is impregnated into a porous TiO_2 structure and compared with a common carbon working electrode (Fig. 5). Both cathode types contain 70 wt% of sulfur and were cycled with a rate of 0.5C as well as 1C. Fig. 5 demonstrates the significant influence of TiO_2 on the cycle dependent electrochemical capacity. The utilization of TiO_2 leads to an observable delayed release of the living phase. This results in an increase in Ref. C_{ec} for the first ten cycles followed by a decrease for higher cycle numbers n . As explained earlier, this specific curve shape is associated to the occurrence of a sleeping phase f_s .

The parameters in Table 1 indicate the diminishing of the unstable living phase $f_{\text{liv}2}$ and an increase in the stable living phase $f_{\text{liv}1}$ accompanied by an occurrence of a sleeping phase. At the same time the conditional transition probability $k_{\text{liv}1 \rightarrow d}$ is decreased. This clearly indicates an improvement of the long-term stability of the Li/S cell. Ding et al. also stated that the successive *in situ* formation of Li_xTiO_2 supports the conductivity of charge carriers e^-/Li^+ . This mechanism could explain the increase of the capacity curve at early cycle numbers and represents therefore the activation of a former inactive (sleeping) fraction.

Seh et al. [26] investigated the influence of sulfur- TiO_2 core–shell structures on the cycle performance of Li/S cells. The applied yolk-shell approach is addressed to the immense volume expansion during the transition of crystalline sulfur to Li_2S of around 80%. If

Table 1

Comparison of system parameters and figures of merit.

#	Sample	ν_s	r_c	$f_{\text{liv}1}$	$f_{\text{liv}2}$	f_s	f_d	$k_{\text{liv}1 \rightarrow d} [10^{-3}]$	$k_{\text{liv}2 \rightarrow d} [10^{-3}]$	$k_{s \rightarrow \text{liv}1} [10^{-3}]$	$n_{1/2}$	\bar{C}_{ec}	C_{tot}
1	MC-MI	70	0.2	0.42	0.20	—	0.38	2.61	35.6	—	122	671	0.82
	NMC-MI	70	0.2	0.51	0.14	—	0.35	1.56	42.9	—	301	702	2.11
	NMC-CO	70	0.2	0.57	0.11	—	0.32	1.01	60.0	—	528	748	4.37
2	w/o PPy	70	0.5	0.42	0.20	—	0.39	4.29	662	—	127	537	0.68
	with PPy	70	0.5	0.59	0.17	—	0.34	2.74	403	—	197	759	1.50
3	C/S	70	1.0	0.24	0.16	0.02	0.58	5.78	68.1	541	51	444	0.23
	coated	70	1.0	0.38	—	0.02	0.60	2.70	—	553	267	471	1.26
	coated	70	0.5	0.38	—	0.12	0.50	2.31	—	238	385	551	2.12
4	C/S	70	0.5	0.36	0.23	—	0.41	0.92	72.4	—	248	552	1.37
	core shell	70	0.5	0.46	0.15	—	0.39	0.69	70.2	—	618	636	3.93
	yolk shell	70	0.5	0.40	0.24	0.18	0.18	0.37	106	24.2	1693	710	12.0
5	CC S60	60	0.2	0.38	0.49	—	0.13	9.64	607	—	30	565	0.17
	SNF S60	60	0.2	0.27	0.56	0.18	0.01	0.36	841	410	2014	527	10.6
	SNF S70	70	0.2	0.33	0.49	0.18	0.00	1.18	733	312	579	621	3.60

$[\nu_s] = \text{wt\%sulfur}$; $[r_c] = 0.465 \text{ mA g}^{-1} \text{sulfur}$; $[\bar{C}_{\text{ec}}] = \text{mAh g}^{-1} \text{sulfur}$; $[C_{\text{tot}}] = 10^5 \text{ mAh g}^{-1} \text{sulfur}$.

#1: Sun et al. [23] – Nitrogen enriched meso-porous carbon and different sulfur loading.

#2: Kazazi et al. [24] – MWCNT/sulfur composites with/without Polypyrrole and different C-rates.

#3: Ding et al. [25] – C/sulfur composites coated with/without TiO₂ and different C-rates.

#4: Seh et al. [26] – Core/shell and yolk/shell sulfur/TiO₂ structure.

#5: Chung et al. [27] – C/sulfur composite and Ni-foam as current collector.

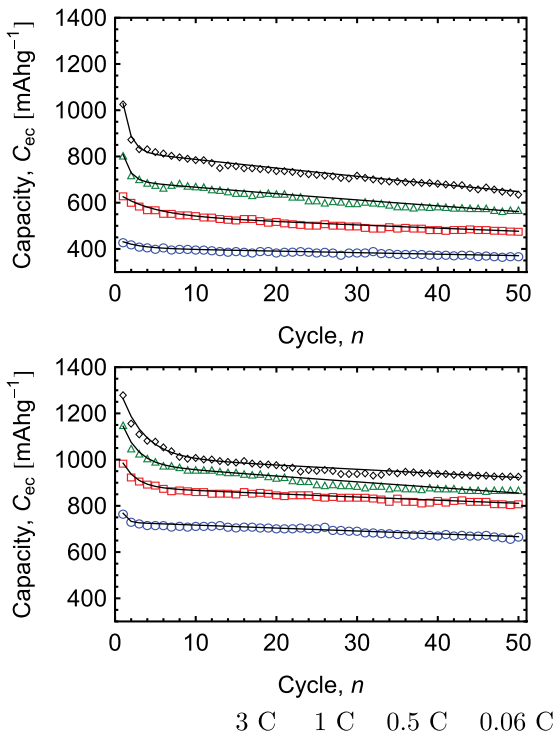
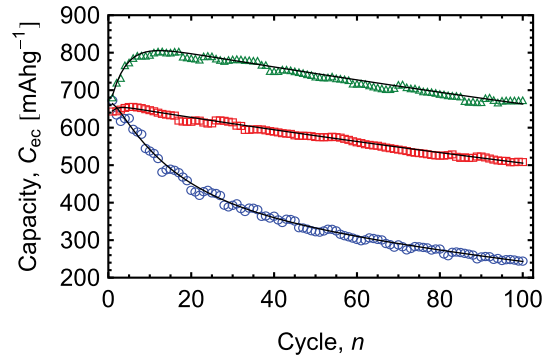
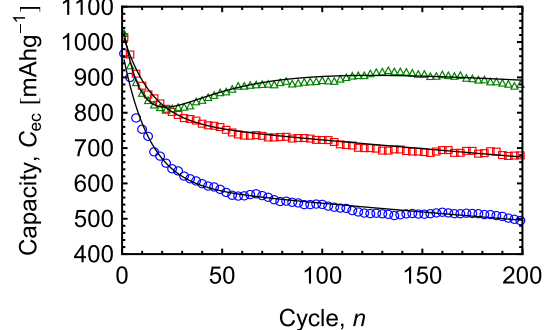


Fig. 4. Cycle dependent electrochemical capacity extracted from the work of Kazazi et al. [24]. Top: w/o PPy coating; Middle: with PPy coating; Bottom: summary of extracted model parameters; Sulfur content 70 wt%, ○:3C, □:1C, ▲:0.5C, ◇:0.06C.

this expansion process is disregarded the TiO₂ shell may be cracked by the sulfur containing core particles. Fig. 6 shows the cycle dependent electrochemical capacities of their investigations. The working electrodes were prepared by mixing the sulfur-based materials with carbon black and PVDF as binder. This results in a sulfur content of approximately 70 wt%. The charge/discharge rate was 0.5C.

Fig. 5. Cycle dependent electrochemical capacity extracted from the work of Ding et al. [25] ○: C/S composite at 1C, □: TiO₂ coated sulfur at 1C, ▲: TiO₂ coated sulfur at 0.5C.Fig. 6. Cycle dependent electrochemical capacity extracted from the work of Seh et al. [26]. Every third cycle is shown. ○: C/S composite, □: core/shell S/TiO₂ structure, ▲: yolk/shell S/TiO₂ structure (parameters extracted from 1000 cycles curve).

The progression of the curves in Fig. 6 is also reflected by the fit parameters in Table 1. The use of a TiO₂ shell results in an increase in the stable living phase $f_{\text{liv}1}$ for core–shell (0.46) and yolk–shell (0.40) particles. Although the value $f_{\text{liv}1}$ of the yolk–shell approach is lower than for core–shell particles, the presence of a sleeping phase yields a better cycle performance for yolk–shell particles. The conditional transition probability $k_{\text{liv}1 \rightarrow d}$ reaches a value of $3.7 \cdot 10^{-4}$ corresponding to a very stable living phase. Thus, this system is very promising for battery applications.

3.3. Metal cathodes

Chung and Manthiram [27] employed porous nickel foam substrates with pore diameters in the range of around 100 μm to achieve bi-functional 3D sulfur–nickel foam cathodes. These special type of cathode material leads to the successful trapping of polysulfides inside the electrode due to the strong chemisorption of the sulfur species with metallic surfaces. Furthermore the nickel foam serves as excellent internal electron transport network. The charge/discharge rate was 0.2C.

The respective capacity fading curves are shown in Fig. 7. While the conventional cathode with 60 wt% sulfur content shows the typical capacity decay for common carbon cathodes, represented by a fast drop (unstable living phase $f_{\text{liv}2}$) followed by a slow decay (stable living phase $f_{\text{liv}1}$), both curves of the cathode made of nickel foam exhibit the presence of a sleeping phase. The sum of stable living and sleeping phase ($f_{\text{liv}1} + f_s$) increases from 0.38 over 0.44 up to 0.51 for conventional, metal/sulfur (60 wt%) and metal/sulfur (70 wt%) cathodes, respectively. More remarkable are the values for the $k_{\text{liv}1 \rightarrow d}$ parameter that represents the long term stability. This value is reduced from $9.6 \cdot 10^{-3}$ to $3.6 \cdot 10^{-4}$ for the conventional and metal/sulfur cathode (60 wt%), respectively (Table 1). This results in a high value of $n_{1/2} = 2014$ and $C_{\text{tot}} = 10.6 \cdot 10^5 \text{ mAh g}^{-1}_{\text{sulfur}}$.

3.4. Comparison between different approaches

There are two main features of the carbon cathodes analyzed herein: First, the absence of a sleeping phase, and second the pronounced presence of an unstable living phase that could possibly be ascribed to the film formation period during the first cycles of the charge/discharge process [5]. Furthermore, the conditional transition probability $k_{\text{liv}1 \rightarrow d}$ that describes the long term stability of a battery ranges from $1.0 \cdot 10^{-3}$ to $4.3 \cdot 10^{-3}$. This results in a maximum half-life cyclability of $n_{1/2} = 528$ cycles with an average capacity output of $\bar{C}_{\text{ec}} = 750 \text{ mAh g}^{-1}_{\text{sulfur}}$.

In case of the cathodes containing metal oxides and metal cathodes we find a sleeping phase. More importantly, there are very

low values of $k_{\text{liv}1 \rightarrow d}$ of $0.37 \cdot 10^{-3}$ and $0.36 \cdot 10^{-3}$, respectively. This feature leads to high values for $n_{1/2}$ and C_{tot} of up to 2000 and $12 \cdot 10^5 \text{ mAh g}^{-1}_{\text{sulfur}}$, respectively. A clear difference between both systems is the value of the conditional transition probability $k_{\text{liv}2 \rightarrow d}$ that determines the kinetic of the film formation period at the beginning of cycling. The cathode which utilizes metal exhibits a $k_{\text{liv}2 \rightarrow d}$ that is one order of magnitude higher than that of metal oxides. This clearly shows a fast decay of the unstable living phase. One possibility for this could be strong adsorption of sulfur species on metal surfaces [28].

Following the quantitative analysis enabled by our new model (Table 1) it appears that approaches utilizing metal oxide and metal cathode present promising routes for further improvements of Li/S cells. In particular, their very low values of conditional transition probabilities $k_{\text{liv}1 \rightarrow d}$ are resulting in convincing figures of merit, and may be regarded as trend-setting for further Li/S battery concepts.

4. Conclusion

A linear four state model with only six fit parameters has been introduced. It describes the cycle-dependent fading of the capacity of Li/S batteries. We demonstrated that the model allows us to obtain excellent agreement with recently published data. This leads to a direct comparison of different concepts of Li/S batteries (see Table 1). Based on our analysis it can be concluded that the presence of metal oxide or metal in the cathode introduces a sleeping phase. This could be attributed to the stronger interaction between metal atoms and sulfur species that is not observed for carbon–sulfur systems. Moreover, the use of metal oxide and metal shows a positive effect on the conditional transition probability $k_{\text{liv}1 \rightarrow d}$ that governs the long-term cycle stability of a lithium sulfur cell. This strongly suggests that the successful trapping of the polysulfides is the result of the strong surface interaction of sulfur and metal. In addition to this, our model provides three figures of merit, namely $n_{1/2}$, \bar{C}_{ec} and C_{tot} . These parameters may be used for a quantitative assessment of novel Li/S-concepts and provide the guidelines for further improvement of a given system.

Acknowledgment

S.A.-U. and J.D. thank the Alexander von Humboldt (AvH) Foundation for financial support.

References

- [1] A. Arico, P. Bruce, B. Scrosati, J. Tarascon, W. Van Schalkwijk, Nat. Mater. 4 (5) (2005) 366–377.
- [2] P. Bruce, S. Freunberger, L. Hardwick, J. Tarascon, Nat. Mater. 11 (1) (2012) 19–29.
- [3] J. Goodenough, Y. Kim, Chem. Mater. 22 (3) (2010) 587–603.
- [4] S. Zhang, J. Power Sources 231 (2013) 153–162.
- [5] P. Arora, R. White, M. Doyle, J. Electrochim. Soc. 145 (10) (1998) 3647–3667.
- [6] P. Ramadass, B. Haran, R. White, B. Popov, J. Power Sources 123 (2) (2003) 230–240.
- [7] R. Spotnitz, J. Power Sources 113 (1) (2003) 72–80.
- [8] P. Ramadass, B. Haran, P. Gomadam, R. White, B. Popov, J. Electrochim. Soc. 151 (2) (2004) A196–A203.
- [9] B. Liaw, R. Jungst, G. Nagasubramanian, H. Case, D. Doughty, J. Power Sources 140 (1) (2005) 157–161.
- [10] Q. Zhang, R. White, J. Power Sources 179 (2) (2008) 793–798.
- [11] O. Erdinc, B. Vural, M. Uzunoglu, in: ICCEP 2009 vols. 1 and 2, 2009, pp. 374–377.
- [12] X. Lin, J. Park, L. Liu, Y. Lee, A.M. Sastry, W. Lu, J. Electrochim. Soc. 160 (10) (2013) A1701–A1710.
- [13] L. Lam, P. Bauer, IEEE T. Power Electr. 28 (12, SI) (2013) 5910–5918.
- [14] Y. Xie, J. Li, C. Yuan, J. Power Sources 248 (2014) 172–179.
- [15] A. Markov, in: Markov Chains, R. Howard (Eds.), Dynamic Probabilistic Systems, vol. 1, John Wiley and Sons, 1971. Appendix B.
- [16] F. Noe, S. Fischer, Curr. Opin. Struct. Biol. 18 (2) (2008) 154–162.

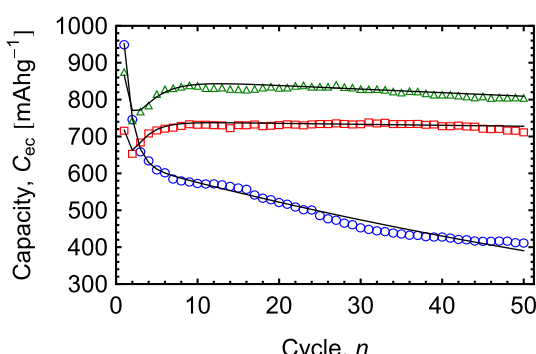


Fig. 7. Cycle dependent electrochemical capacity extracted from the work of Chung et al. [27]; ○: CC-S60 – conventional cathode with 60 wt% sulfur; □: SNF cathode with 60 wt% sulfur; △: SNF cathode with 70 wt% sulfur.

- [17] F. Noe, J. Chem. Phys. 128 (24) (2008) 244103.
- [18] S. Bashash, S. Moura, H. Fathy, J. Power Sources 196 (2011) 8747–8754.
- [19] N. Michelusi, L. Badia, R. Carli, L. Corradini, M. Zorzi, in: IEEE Infocom, 2013, pp. 590–594. Article number 6566841.
- [20] G. Yu, L. Sheng, M. Guo, in: Applied Mechanics and Materials Vol. 378, 2013, pp. 492–495.
- [21] J. Song, V. Krishnamurthy, A. Kwasinski, R. Sharma, IEEE T. Sustain Energy 4 (2) (2013) 491–500.
- [22] S. Moura, J. Stein, H. Fathy, in: IEEE Transactions on Control Systems Technology Vol. 21, 2013, pp. 679–694. Article number 6175937.
- [23] F. Sun, J. Wang, H. Chen, W. Qiao, L. Ling, D. Long, Sci. Rep. 3 (2013) 1–8.
- [24] M. Kazazi, M. Vaezi, A. Kazemzadeh, Ionics.
- [25] B. Ding, L. Shen, G. Xu, P. Nie, X. Zhang, Electrochim. Acta 107 (2013) 78–84.
- [26] Z. Seh, W. Li, J. Cha, G. Zheng, Y. Yang, M. McDowell, P. Hsu, Y. Cui, Nat. Comms. 4 (2013) 1–6.
- [27] S. Chung, A. Manthiram, Electrochim. Acta 107 (2013) 569–576.
- [28] J. Rodriguez, J. Hrbek, Acc. Chem. Res. 32 (9) (1999) 719–728.
- [29] N. van Kampen, Stochastic Processes in Physics and Chemistry, third ed., North Holland, 2007.
- [30] G. Allen, Lectures on Linear Algebra and Matrices, A & M University, Texas, 2003.